THE JOURNAL OF BIOLOGICAL CHEMISTRY
Vol. 278, No. 26, Issue of June 27, pp. 23251–23259, 2003
Printed in U.S.A.

Bacillus subtilis Bacteriophage SPP1 DNA Packaging Motor Requires Terminase and Portal Proteins*

Received for publication, February 20, 2003, and in revised form, April 11, 2003
Published, JBC Papers in Press, April 14, 2003, DOI 10.1074/jbc.M301805200

Ana G. Camacho‡§, Aranzazu Gual‡, Rudi Lurz¶, Paulo Tavares‖, and Juan C. Alonso‡

From the ‡Departamento de Biotecnología Microbiana, Centro Nacional de Biotecnología, Consejo Superior de Investigaciones Científicas, Campus Universidad Autónoma de Madrid, Cantoblanco, 28049 Madrid, Spain, the ¶Max-Planck-Institut für molekulare Genetik, Ihnestrasse 73, D-14195 Berlin, Federal Republic of Germany, and the ‖Unité de Virologie Moléculaire et Structurale, Bâtiment 14B, CNRS, 91198 Gif-sur-Yvette, France

Initiation of headful packaging of SPP1 DNA concatemers involves the interaction of the terminase, G*1*P and G*2*P, and the portal protein, G*6*P. G*1*P, which specifically recognizes the non-adjacent *pac*L and *pac*R subsites and directs loading of G*2*P to *pac*C, interacts with G*6*P. G*2*P, which has endonuclease, DNA binding, and ATPase activities, interacts with G*1*P and does it transiently with G*6*P. The stoichiometry of G*1*P on the G*1*P·G*2*P complex promotes the transition from a G*2*P endonuclease to an ATPase. G*6*P does not alter the endonuclease activity of G*2*P. Both G*1*P and G*6*P, which do not have endogenous ATPase activity, synergistically enhance and modulate the ATPase activity of G*2*P. Based on these results, we propose a model in which the modulation of the ATPase and endonuclease activities of G*2*P accounts for the role of the terminase in headful packaging.

Many cellular processes require the action of a biological motor protein that converts chemical energy into mechanical force or directional movement. Packaging of viral head-to-tail concatemeric dsDNA[1] into viruses involves the specific interaction of virus DNA with the pre-assembled procapsid and subsequent translocation of the former into the latter, by the action of a DNA translocase, to render a highly condensed structure (1–4). DNA translocases are molecular motor proteins that use the energy of nucleoside triphosphate hydrolysis to package concatemeric dsDNA onto an empty procapsid. This is a common feature shared by the DNA packaging machinery of many bacterial, pox, and herpes viruses. Two general modes for packaging of concatemeric dsDNA into the capsid of a bacterial virus (also termed bacteriophage or phage) have been proposed. The first implies a site-specific packaging in which the recognition sequence (termed *cos* in phage λ) plays an important role in initiation and termination of DNA encapsidation. This packaging process, which generates unit-length encapsidated molecules, is well characterized in phages λ, T3, and T7 (1–4). The second mode implies headful packaging, in which the encapsidation initiates at a specific site in the genome (termed *pac* in phage SPP1), but with the capacity of the procapsid playing a predominant role in the termination step. The sequential headful packaging mechanism generates a heterogeneous population of terminally redundant and partially circularly permuted DNA molecules as in the cases of SPP1, P1, P22, or in the case of T4 whose DNA is totally permuted and terminally redundant (Refs. 1 and 3 and Fig. 1).

Bacillus subtilis phage SPP1 replication results in the formation of large head-to-tail concatemeric dsDNA. To initiate DNA packaging, the terminase, composed of small G*1*P and large G2P subunits, recognizes and cleaves the concatemeric DNA within the *pac* site (see Refs. 5 and 6 and Fig. 1). The SPP1 packaging site is divided into three discrete subsites: *pac*L, defining the non-encapsidated or left DNA end, *pac*C, the cleavage site, and *pac*R, the encapsidated or right DNA end (Refs. 7 and 8 and Fig. 1*A*). The terminase, bound to the encapsidated DNA end, interacts with the portal protein G*6*P. Then, the DNA is translocated into an empty procapsid until the head is full (5, 7, 9). Viral DNA translocation is a poorly understood mechanism. The SPP1 packaging motor lies at a unique vertex of the procapsid and contains the hetero-oligomeric SPP1 terminase enzyme, composed of two decameric ring-shaped G*1*P and two monomeric G2P, which assemble onto the *pac* site of SPP1 concatemeric linear dsDNA molecule, and the oligomeric G*6*P composed of 12 identical subunits (6, 8, 10). However, purified G*6*P in solution has 13 subunits (11). Unless otherwise stated, G*1*P is expressed as a protein decamer, G2P as a monomer, and G*6*P as a tridecamer.

G*1*P specifically recognizes the a-boxes at the *pac*L subsite and wraps it and contacts the c-boxes at the *pac*R subsite (Refs. 7 and 8 and Fig. 1*A*). One G*1*P protein bound to *pac*L and another bound to *pac*R subsites interact and hold the two subsites together in a DNA loop containing the *pac*C subsite (8). G*1*P introduces a DNA distortion in the *pac* region, loads one G2P monomer at each of the b-boxes (Refs. 6, 8, and 12 and Fig. 1*A*), and interacts with G*6*P (this work). G2P possesses an ATP-independent endonuclease, a weak ATPase, and a sequence-independent DNA binding activity. The terminase with a relative stoichiometry of one G*1*P and one G2P has a very weak ATPase and an active ATP-independent endonuclease activity. However, at a higher G*1*P ratio the terminase enzyme binds DNA, is an active ATPase, and has a very poor endonuclease activity (Refs. 5, 6, 8, and 13 and this report). These properties suggested a mechanism for terminase function in the specific recognition and cleavage of the *pac* sequence within the viral DNA that initiates DNA packaging (5, 6). The terminase, perhaps with the $G1P_1 \cdot G2P_1$ stoichiometry, introduces a 1-bp staggered cut at each of the 10-bp b-boxes (5′-CTATTGCGG↓C-3′, see Fig. 1*A*) within the distorted *pac*C subsite or less specific cuts with a certain preference at the

* This work was partially supported by Grants BMC2003-00150 and BIO2001-4339-E from Dirección General de Investigación, Ministerio de Ciencia y Tecnología (to J. C. A.). The costs of publication of this article were defrayed in part by the payment of page charges. This article must therefore be hereby marked "*advertisement*" in accordance with 18 U.S.C. Section 1734 solely to indicate this fact.

§ Recipient of a Fellowship of the Consejeria de Educación y Cultura-Comunidad de Madrid (0381/1999).

** To whom correspondence should be addressed. E-mail: jcalonso@cnb.uam.es.

[1] The abbreviations used are: dsDNA, double-stranded DNA; Myr, myricetin; SSR, square summatory residual.

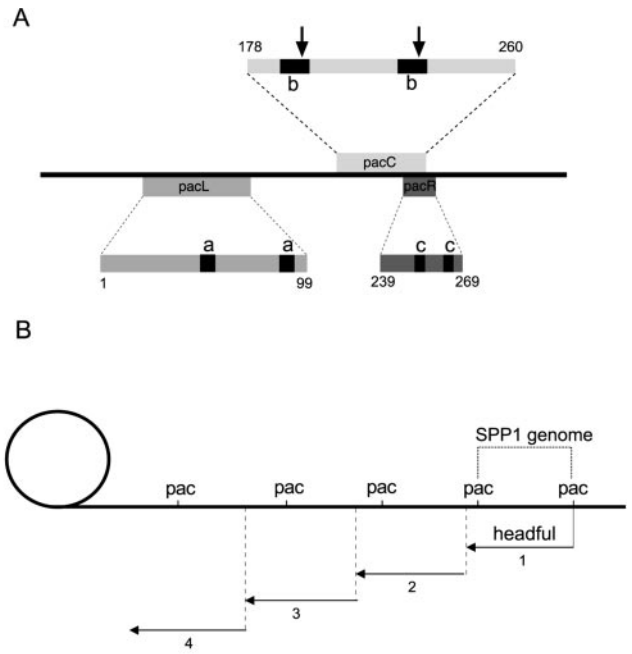

FIG. 1. **The *pac* region of bacteriophage SPP1.** *A*, the *bar* indicates the SPP1 DNA. The *pac*L (non-encapsidated left end), *pac*R (encapsidated right end) and *pac*C (the processing site) are enlarged. The filled 7-bp *boxes a* and *c*, which are recognized by G*1*P, and the 10-bp *boxes b*, to which G2P introduces staggered cuts (denoted by *arrows*), are labeled. *B*, a concatemeric DNA substrate of SPP1 for the headful packaging mechanism. The region of DNA contained between two *pac* sites corresponds to unit-length SPP1 genome (44.6 kb). Initiation of SPP1 packaging occurs at a unique *pac* site until the head is full (mature chromosome size is 45.9 kb). The terminal redundancy (about 3%) is generated by the imprecise headful cuts. The *pac* site is used only once per packaging series (4 packaging events).

5′-GG ↓ CW-3′ sequence at any other DNA sequence (6, 12–14). Upon cleavage at *pac*C, the DNA end proximal to *pac*L is degraded by the G2P endonuclease (5, 6). We have proposed that the G*1*P molecule bound to *pac*L and interacting with the other G*1*P molecule bound to *pac*R is now free to interact with G2P that has cleaved the b-box proximal to *pac*R (Refs. 5 and 6 and Fig. 1*A*). The terminase with a $G1P_{>1}$·$G2P_1$ stoichiometry protects the DNA end proximal to *pac*R, the endonuclease activity is shut off, and the ATPase activity increases (this work). The DNA binding activity of G2P remains unchanged (6). ATPase activity is associated exclusively to G2P as G*1*P binds but does not hydrolyze ATP (6). Like G*1*P, the ring-shaped oligomeric small subunit of phage T4 terminase (gp16) also enhances the ATPase activity of the monomeric terminase large subunit (15–17).

The current packaging model predicts that the DNA end bound to the terminase is translocated unidirectionally into a preformed procapsid through a specialized channel provided by the portal protein, G*6*P, in an ATP-driven reaction. When a threshold amount of DNA, representing ~103% of the genome, has been packaged the terminase introduces a poor sequence-specific cut (headful cut), perhaps at the 5′-GG ↓ CW-3′ sequence, that terminates the encapsidation cycle. A second cycle of encapsidation initiates from the terminase generated end, and sequential headful packaging events proceed along the DNA concatemer in a processive fashion (Refs. 5, 6, 7, 13, and 18 and Fig. 1*B*).

The mechanism by which packaging translocases couple the NTPase activity with dsDNA movement is still unclear and remains a subject of intense study. The SPP1 terminase and portal protein show sequence similarity with equivalent proteins from other phages that infect Gram-positive bacteria. Furthermore, G2P shows ~30% identity within a 75-residue long segment with the SecA translocase, an RNA helicase, and with proteins involved in lipid transport (data not shown).

In this report we have analyzed the interaction of purified terminase with the portal protein. Using different methods we might infer that G*1*P interacts with G*6*P. Initial velocity studies were performed in order to determine kinetic constants to define the influence of these two proteins over the ATPase activity of G2P. On the basis of the data obtained, a model for assembly and interaction of the terminase subunits with the portal protein to promote DNA translocation is presented.

EXPERIMENTAL PROCEDURES

Enzymes and Reagents—G*1*P, G2P, and G*6*P were purified as previously described (12, 6, 11). The concentration of proteins was determined by UV absorbance at 280 nm as previously described (6). G*1*P, G2P, and G*6*P concentrations are expressed as mole of protein decamers, monomers, and 13-mers, respectively. Covalently closed circular plasmid DNA pBT363-borne *pac* DNA was purified by using the SDS lysis/cesium chloride/ethidium bromide gradient method (12).

[γ-^{32}P]ATP and glutaraldehyde were purchased from Amersham Biosciences. Myr, proteinase K, and anti-rabbit IgG were purchased from Sigma. Polyclonal antibodies against G*1*P and G*6*P were previously used (18, 19). Glycerol was purchased from ICN, Biomedicals Inc., Trizma base was from Biomedicals, Nitro-Block™ was from Tropix. Imidazole and trichloroacetic acid were purchased from Merck.

Glycerol Gradient—G*1*P (4 μM) and G*6*P (3 μM) were preincubated in buffer A (50 mM Tris-HCl, pH 8), containing 10 mM $MgCl_2$ and 300 mM or 50 mM NaCl, over 15 min at 30 °C, loaded onto the gradient (10–30%), and centrifuged (SW50 Ti, 45,000 rpm, 6 h at 4 °C). The aliquots taken from the bottom of the tubes were separated by 15% (w/v) SDS-PAGE, electroblotted onto polyvinylidene difluoride Immobilon-P transfer membrane (Millipore) according to standard procedures, and the proteins detected by a mixture of polyclonal antibodies raised against both proteins. The signals were quantified by laser densitometric scanning.

ATPase Assay—Standard reactions were incubated in buffer B (50 mM Tris-HCl, pH 7.5 containing 10 mM $MgCl_2$, 50 mM NaCl, and 1 mM dithiothreitol) in a final volume of 20 μl. The reactions were initiated by addition of the substrate after a preincubation of the proteins for 5 min at 37 °C and were allowed to proceed for 15 min more at 37 °C. ATPase activity was determined by measuring the amount of phosphate set free upon hydrolysis as previously described (21). Initial velocity studies were performed using 20 nM of G2P and an ATP concentration range of 0.0005–10 mM (10–0.05 μCi/nmol). The initial velocity of ATP hydrolysis was determined within the linear range of each reaction using the following protein concentrations: 20 nM G2P, 95 nM G*1*P, and 80 nM G*6*P.

ATP hydrolysis in the presence of different concentrations of G*6*P or/and G*1*P proteins and Myr, was carried out with 5 mM [γ-^{32}P]ATP, 0.05 μCi/nmol. K_m and V_{max} values were obtained by non-linear least-squares fit of the experimental data to the Michaelis-Menten equation with the Kaleidagraph© version 3.0.2 Abelbeck Software program. The mathematics software, MATLAB® version 5.1, has made possible an iterative analysis to fit the experimental data with several theoretical models.

For the binary interaction of G2P-G*1*P and G2P-G*6*P (see Fig. 3), considering *E*, the enzyme (G2P); *M*, the modulator (G*1*P or G*6*P); α, the ratio between $[EM_\alpha]$ and $[E]_0$; *a*, the modulator stoichiometry coefficient; and x_0, the ratio between $[M]_0$ and $[E]_0$, Equations 1 and 2 were applied.

$$K[E]_0^a = \frac{\alpha}{(1-\alpha)(x_0 - a\alpha)^a} \quad \text{(Eq. 1)}$$

$$r_0 = V_{max_E}(1-\alpha) + V_{max_{EM_a}}\alpha \quad \text{(Eq. 2)}$$

For the ternary interactions (Fig. 4): G2P-G*1*P-G*6*P, x_0 corresponds to the ratio between $[G1P]_0$ and $[G2P]_0$, and y_0 corresponds to the ratio between $[G6P]_0$ and $[G2P]_0$. The applied Equations 3–6 were as follows.

$$x_0 = x + \frac{K_{B3}[C1]_0 xy_0}{(1 + K_{B3}[C1]_0 x)} + \frac{(2K_{A1}([C1]_0)^2 x^2 + 4K_{B1}([C1]_0)^4 x^4)}{(1 + K_{A1}([C1]_0)^2 x^2 + K_{B1}([C1]_0)^4 x^4)} \quad \text{(Eq. 3)}$$

$$r_0 = \frac{V_{\max_{C1}} + V_{\max_A} K_{A1}([C1]_0)^2 x^2}{1 + K_{A1}([C1]_0)^2 x^2 + K_{B1}([C1]_0)^4 x^4} \quad \text{(Eq. 4)}$$

$$y_0 = y + \frac{K_{B3}[C2]_0 y x_0}{(1 + K_{B3}[C2]_0 y)} + \frac{(K_{A2}[C2]_0 y + 2K_{B2}([C2]_0)^2 y^2)}{(1 + K_{A2}[C2]_0 y + K_{B2}([C2]_0)^2 y^2)} \quad \text{(Eq. 5)}$$

$$r_0 = \frac{V_{\max_{C2}} + V_{\max_A} K_{A2}[C2]_0 y}{1 + K_{A2}[C2]_0 y + K_{B2}([C2]_0)^2 y^2} \quad \text{(Eq. 6)}$$

Endonuclease Activity Assay—The concentration of DNA was determined by using molar extinction coefficients of 6,500 $M^{-1} \times cm^{-1}$ at 260 nm. Form I pBT363 (20 nM) was incubated with G2P (80 nM) and different concentrations of G*1*P and G*6*P over 60 min at 37 °C in buffer C (50 mM Tris-HCl, pH 7.5, 50 mM NaCl, 10 mM $MgCl_2$). G2P exhibited endonuclease activity that converted Form I or supercoiled into Form II or open circular DNA as well as Form III or linear DNA (6). The conversion from Form I into Form II plus Form III DNA Forms was measured. In the experiments with Myr, the inhibitor was used at 0.5, 1, 5, 10, 20, and 50 μM concentrations. When G*1*P was included in the reaction Myr at 160 nM was used. Reactions were stopped by addition of 50 mM EDTA, samples deproteinized by incubation with proteinase K, and addition of 1% SDS over 30 min at 37 °C. Analytical gel electrophoreses were carried out in 0.8% (w/v) agarose/Tris borate-EDTA/ethidium bromide horizontal slab gels.

Protein-Protein Interaction Assay—For protein cross-linking, the pure proteins were incubated in the presence of 0.04% glutaraldehyde at room temperature in buffer D (60 mM Na_2HPO_4, pH 7.2) containing 30 mM $MgCl_2$, 50 mM NaCl, and 1.5 mM dithiothreitol with and without 1–50 μM Myr. Aliquots were collected at different times, and the reactions were stopped by precipitating the proteins with 25% (w/v) trichloroacetic acid, followed by two washing steps with acetone. The pellets were dissolved in cracking buffer and loaded on a 15% SDS-PAGE.

RESULTS

G1P Physically Interacts with G6P—Previously, it has been shown that G2P interacts with G*1*P (19, 6), but fails to form a stable complex with G*6*P (23, 19, 6). To learn whether G*1*P interacts with G*6*P a glycerol gradient was used. G*1*P (predicted molecular mass of 20.7 kDa), and the portal protein, G*6*P (predicted molecular mass of 57.3 kDa), have native molecular masses of 210 kDa (10 mer) and 745 kDa (13 mer), respectively (see Refs. 5, 8, 11, and 22). G*1*P (4.5 μM), G*6*P (2.9 μM), or both proteins in buffer A containing 50 or 300 mM NaCl were loaded onto a linear glycerol gradient and centrifuged. The aliquots, collected from the bottom of the tube, were separated by SDS-PAGE, electroblotted, and revealed by Western blot analysis. When the collected fractions were analyzed, a G*6*P broad peak, with a maximal protein concentration between fractions 4 and 5, was observed (Fig. 2*A*), whereas a sharper peak, with maximal protein concentration between fractions 7 and 9, was detected for G*1*P (Fig. 2*B*).

The sedimentation coefficients corresponding to a molecular mass of 600–800 kDa for G*6*P (Fig. 2*A*) and of ~200 kDa for G*1*P were calculated (Fig. 2*B*). In the presence of 300 mM NaCl, the G*6*P and G*1*P peaks are similar to the ones corresponding to the individual proteins (Fig. 2*C*). In the presence of 50 mM NaCl, however, G*1*P shifted from fractions 7–9 to fractions 2–4, and G*6*P was observed between fractions 2 and 5. The estimated native mass of protein complex present in fraction 3 should be ~1,000 kDa (Fig. 2*D*). Furthermore, protein-protein cross-linking followed by immunoprecipitation allowed us to pull-down both G*1*P and G*6*P proteins (data not shown). These results are consistent with electron microscopy studies. Preliminary results, albeit with a limited resolution of the electron micrographs, suggest that G*1*P binds to the stem domain of G*6*P in several visualized structures.[2] Since the G*6*P stem domain faces the capsid exterior (see Refs. 10 and 24) it is likely

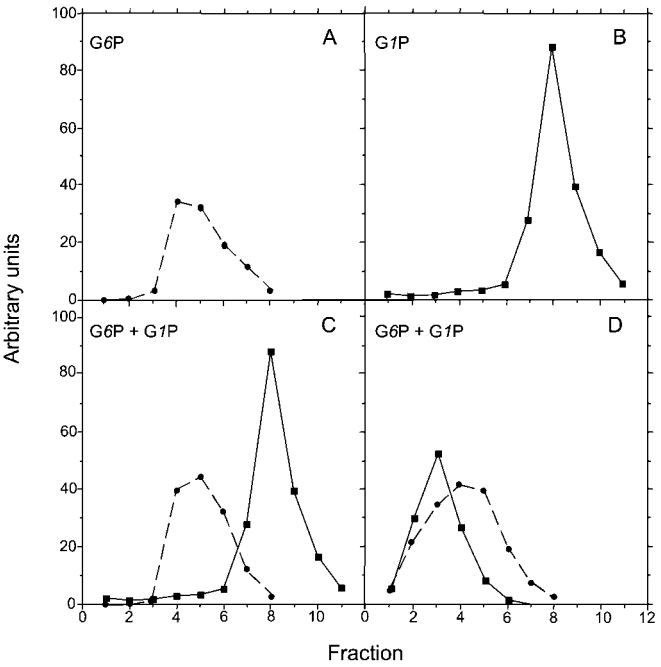

FIG. 2. **Glycerol gradient of G*1*P and G*6*P.** *Panels A* and *B* correspond to sedimentation profiles of proteins G6P (*filled circles* joined by a *broken line*) and G*1*P (*filled squares* joined by a *straight line*), respectively, in buffer A containing 300 mM NaCl. *Panels C* and *D* correspond to the sedimentation profiles of both proteins together in buffer A containing 300 and 50 mM NaCl, respectively.

that the detected interaction, both in the absence of G2P and/or DNA, is relevant.

G6P and G1P Enhance Synergistically the G2P ATPase Activity—G2P hydrolyzed ATP and dATP to the corresponding diphosphate and inorganic phosphate, with a low affinity (K_m, ~950 μM) and activity (k_{cat}, 26 ± 1 min^{-1}), but fails to hydrolyze other NTPs and dNTPs (6). To address whether G*6*P is able to interact and modify any of the G2P activities, we incubated both proteins and performed nuclease and ATPase assays. G*6*P does not have a nuclease or NTPase activity of its own (data not shown). As revealed in Table I, G*6*P is able to enhance ~2-fold the G2P ATPase activity but does not seem to modify the G2P nuclease activity (see below). The effect of G*6*P in lowering the K_m and increasing k_{cat} of the G2P ATPase is specific because neither bovine serum albumin nor a heat-inactivated G*6*P is able to stimulate the ATPase activity of G2P (data not shown).

Previously, it has been shown that G*1*P lowers the K_m and increases the k_{cat} of the G2P ATPase (Ref. 6 and Table I). The presence of both G*6*P and G*1*P increase the G2P ATPase or dATPase activity, regarding both the K_m of the substrate and the reaction velocity of the enzyme. None of the other purified components of the SPP1 procapsid (major capsid protein, G*13*P, scaffolding protein, G*11*P, and accessory protein, G7P) affect the ATPase activity of G2P (23).

In the G2P ATPase activity, ATP behaved as a Michaelis-Menten type substrate (see Table I). The K_m and V_{max} values were obtained by non-linear least-squares fit of the experimental data to the Michaelis-Menten equation. Since we have failed to detect a stable G2P·G*6*P complex by affinity chromatography, we assumed that G*6*P might form a transient complex with G2P. It is likely, therefore, that G*6*P forms a complex with the terminase (G*6*P·G*1*P·G2P), and that G*6*P couples the stimulated ATPase to the functional SPP1 DNA packaging machinery.

G2P Interacts with G6P with a $G6P_1 \cdot G2P_1$ Stoichiometry—The ATPase activity of the G2P enzyme (*E*) in the presence of

[2] R. Lurz and A. G. Camacho, unpublished results.

TABLE I
Catalytic parameters of G2P, G1P·G2P, G2P·G6P and G1P·G2P·G6P

Protein added	K_m	V_{max}	k_{cat}	k_{cat}/K_m
	μM	$\mu mol\ min^{-1}\ mg^{-1}$	min^{-1}	$M^{-1}\ s^{-1}$
G2P[a]	913 ± 52	0.5 ± 0.01	25	4.5×10^2
G2P + G1P	324 ± 81	1.7 ± 0.1	83	4.3×10^3
G2P + G6P	605 ± 80	1.0 ± 0.2	47	1.3×10^3
G2P + G1P + G6P	219 ± 25	6.4 ± 1.2	305	2.3×10^4

[a] ATPase assay was performed at 37 °C. Time was fixed depending on the substrate concentration used in order to maintain the hydrolysis within the linear range of each reaction. k_{cat} was determined considering V_{max} values obtained by non-linear least-squares fit of the experimental data to the Michaelis-Menten equation and a G2P concentration of 20 nM.

increasing concentrations of G6P modulator (*M*) was analyzed using a mathematical program (see "Experimental Procedures"). This program made possible an iterative analysis to fit the experimental data with several theoretical models (one G2P with one, two, or three G6P molecules, E_1M_1, E_1M_2, E_1M_3, etc).

The values of the catalytic constants were obtained by non-linear least-squares fit of the experimental data to the Michaelis-Menten equation in the presence of increasing ATP concentrations. ATPase assays were performed with a constant amount of G2P and increasing G6P concentrations. The experimental data suggest that the stoichiometry of the complex fits best with the theoretical E_1M_1 model, which corresponds to the lowest SSR value, with a very high constant of 1.58 nM^{-1}. It is noteworthy that this very high value for *K*, suggests a tendency for G2P to be in a complex with G6P with a 1:1 stoichiometry (Fig. 3*A*). When experiments containing a constant amount of G6P and increasing G2P concentrations were performed, a peak corresponding to a 1:1 stoichiometry was obtained, supporting the above data (data not shown). Since, there is only one G6P oligomer per empty procapsid it is likely that the stoichiometry of G2P and G6P in the packaging complex is $G2P_1{\cdot}G6P_1$.

G2P Interacts with G1P with a $G1P_{2-3}{\cdot}G2P_1$ Stoichiometry—G1P enhances the G2P ATPase activity (Ref. 6 and Table I). The ATPase assay was used to measure the stoichiometry of the G1P·G2P complex. As described in the previous section, the assay was carried out with a constant amount of G2P (*E*) and increasing G1P (*M*) concentrations. Initially, three possibilities have been considered (*e.g.* E_1M_1, E_1M_2, E_1M_3). The best fit (the lowest SSR value) corresponds to a stoichiometry coefficient of the modulator (a) = 2 ($K = 6.12 \times 10^{-4}\ nM^{-2}$) or ($a$) = 3 ($K = 4.0 \times 10^{-5}\ nM^{-3}$) and a stoichiometry of $G1P_2{\cdot}G2P_1$ or $G1P_3{\cdot}G2P_1$ (Fig. 3*B*). Since, in the packaging initiation complex there are two decameric G1P bound to the *pac*L and *pac*R DNA loop and one monomeric G2P molecule to the b-box proximal at *pac*R, it is likely that the stoichiometry of the active ATPase complex is $G1P_2{\cdot}G2P_1$ (8, 6). This is consistent with the observation that the second monomeric G2P protein, that degrades the non-encapsidated, leaves the packaging initiation complex (5, 6).

G1P and G6P Modulate G2P Activities—To study the G6P·G1P·G2P complex interaction, two sets of experiments were performed. First, constant G2P and G6P concentrations were incubated with increasing concentrations of G1P and, second, constant G2P and G1P were incubated with increasing concentrations of G6P, and ATPase and nuclease assays were performed. The G6P and G1P concentrations selected suggest that in the initial moment all the G2P molecules would be in the form of the corresponding adducts ($G2P_1{\cdot}G6P_1$ or $G2P_1{\cdot}G1P_2$). As revealed in Fig. 4*A*, a sharp peak corresponding to the first set of experiments, suggests that initially a very active species is formed when G1P is present in the reaction; however, when more G1P is added, the initial active adduct is transformed to a nearly inactive one. Such a negative effect on the ATPase activity is not observed when G6P is omitted from the reaction mixture (Ref. 6 and data not shown). Concerning the G2P endonucleolytic activity, there is a constant inhibition

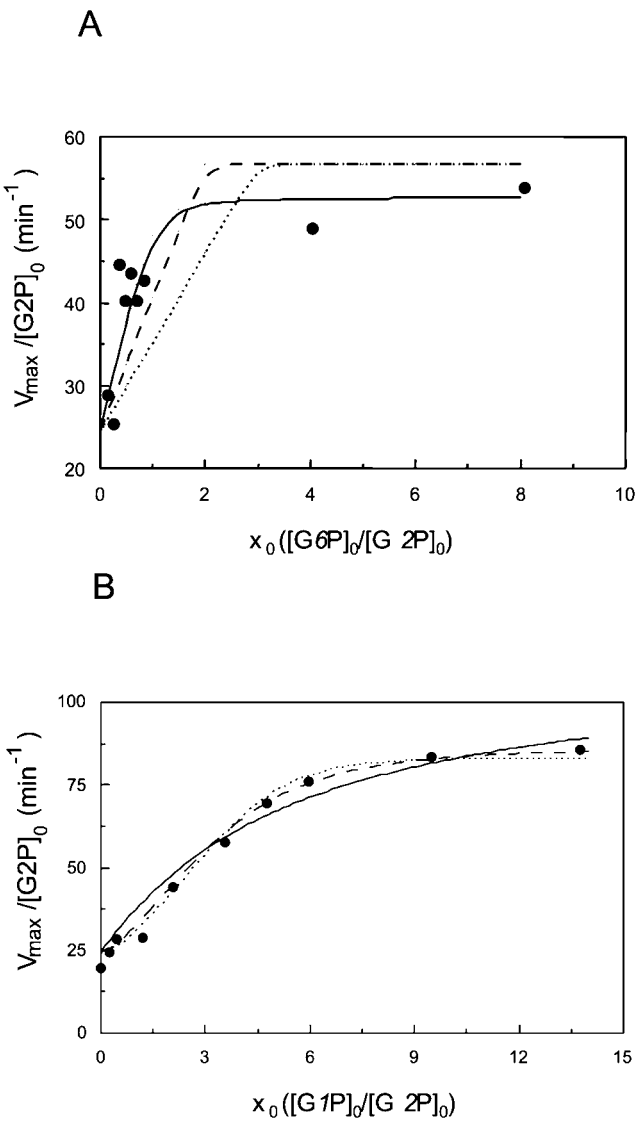

FIG. 3. **Stoichiometry of ATPase complexes.** A comparison of experimental data and theoretical models, revealed different possible stoichiometries. The SSR value shows the deviation of the experimental data regarding each theoretical model. The experimental (*filled circles*) and theoretical (a = 1 (*solid line*); a = 2 (*broken line*), and a = 3 (*dotted line*)). x_0 or y_0 means the ratio between initial concentrations. *A*, the ATPase activity of G2P (20 nM) in the presence of increasing concentrations of G6P (2.5, 5, 7, 9.4, 11.7, 14, 16.4, 80.5, and 161 nM). SSR values are as follows: a = 1, SSR = 0.0823; a = 2, SSR = 0.206; a = 3, SSR = 0.324. *B*, the ATPase activity of G2P (20 nM) in the presence of increasing concentrations of G1P (5, 9, 24, 42, 71, 95, 120, 190, and 275 nM). SSR values are as follows: a = 1, SSR = 0.077; a = 2, SSR = 0.019; a = 3, SSR = 0.023.

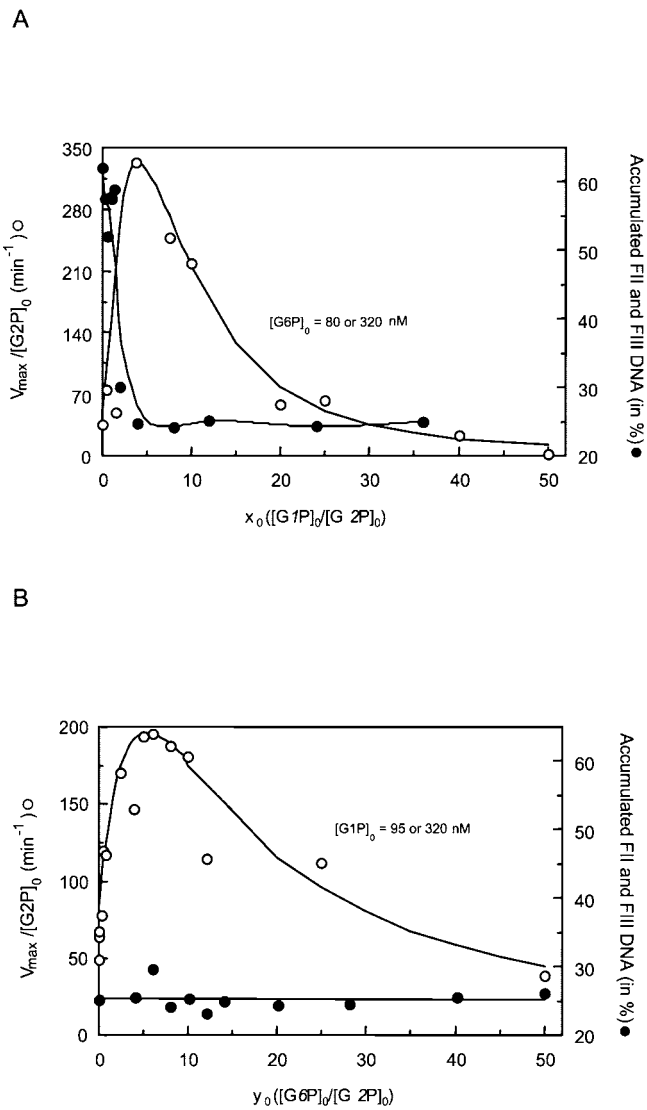

FIG. 4. **G2P ATPase and nuclease activities in presence of both G1P and G6P.** ATPase (*empty circles*) assays were performed with 5 mM ATP (0.05 μCi/nmol). Supercoiled pCB363 DNA (20 nM) was the substrate for the nuclease assay (*filled circles*). *A*, constant amounts of G2P (20 and 80 nM) and G6P (80 or 320 nM) for the ATPase and endonuclease activities, respectively, were incubated with increasing G1P concentrations (10, 30, 75, 150, 200, 400, 500, 900, and 1,000 nM for ATPase and 24, 48, 76, 80, 106, 160, 320, 640, 960, 1,920, and 2,880 nM for endonuclease assays) and the assays carried out. *B*, constant amount of G2P (20 and 80 nM) and G1P (95 and 320 nM) for the ATPase and endonuclease activities, respectively, were incubated with increasing G6P concentrations (0.3, 1.2, 5.5, 10, 16, 50, 80, 100, 121, 162, 200, 242, 500, and 1,000 nM for ATPase and 161, 322, 483, 644, 805, 966, 1,127, 1,288, 1,610, 2,254, and 3,220 nM for the endonuclease activity) and the assays carried out. x_0 or y_0 mean the ratio between initial concentrations.

when G1P is present at a ratio higher than $G1P_{>1}$·$G2P_1$ (Ref. 6 and Fig. 4*A*).

At low G6P, a sharp increase in the ATPase of G2P suggests that initially a very active ATPase species is formed, whereas at higher G6P concentrations, a decreased G2P ATPase is observed (Fig. 4*B*). The presence of an excess of G6P cannot reverse the negative effect of G1P on the G2P endonuclease activity (Fig. 4*B*), suggesting formation of a ternary complex of the three proteins.

The results presented from both series suggest a very active ATPase species, which disappears and is transformed in other inactive or nearly inactive new species in the presence of an excess of any of the modulators (G1P or G6P). Moreover, the possible interaction of both modulators (see Fig. 2), in the absence of G2P, would be a non-catalytic adduct ($G1P_1$·$G6P_1$) that might contribute to the delay of the negative effect of G1P in ATPase activity from the first set of experiments, due to the excess of G6P used. It would be the same in the second set due to the excess of G1P in the initial moment of the reaction. The high number of parameters required to take into account the equilibrium regarding all the existing species make difficult the exact quantitative determination of these constants, although it is indubitable from the experimental data, that these species or other equivalents are formed. All the equilibrium constants of the species formed are summarized in Table II. Moreover, the experiments performed clearly show that the adduct A: $G2P_1$·$G1P_2$·$G6P_1$, formed when the three proteins are in the reaction mixture, presents the highest ATPase activity with a kinetic constant of 366 min^{-1}.

TABLE II
Equilibrium constants of the interaction between the terminase subunits and the terminase and portal protein

For the ternary interaction, G6P·G1P·G2P, we assumed that in the initial moment, the species formed are the ones shown in the binary interactions. We consider: C_1 = $G2P_1$·$G6P_1$ and C_2 = $G2P_1$·$G1P_2$, and the following equilibriums: C_1 + 2 G1P ↔ A_1, C_2 + G6P ↔ A_2, G1P + G6P ↔ B_3; C_1 + 4 G1P ↔ B_1, and C_2 + 2 G6P ↔ B_2. Therefore, the corresponding equilibrium constants should be: K_{A1}, K_{A2}, K_{B3}, K_{B1}, and K_{B2}. The kinetic constant for the most active ATPase species is shown.

First interaction constants		Second interaction constants	
K_{A1}	1.2×10^{-2} nM^{-2}	K_{A2}	1.5×10^{-2} nM^{-1}
K_{B1}	4.7×10^{-7} nM^{-4}	K_{B2}	7.5×10^{-5} nM^{-2}
K_{B3}	10^{-3} nM^{-1}	K_{B3}	10^{-3} nM^{-1}
k_{catA}	366 min^{-1}	k_{catA}	366 min^{-1}

Myricetin Alters G2P Activities—The phosphoinositide 3-kinase protein has been co-crystallized with its inhibitor Myr. Myr in the Myr-phosphoinositide 3-kinase co-crystal fits and fills the ATP binding pocket (25). Furthermore, Myr blocks ATP hydrolysis and DNA translocation in certain DNA helicases (26). To determine whether Myr has any effect on the G2P activities, these assays were performed in the presence of increasing concentrations of Myr. The same Myr (~15 μM) concentration reduces ~50% of the ATPase activity of the G2P·G1P, G2P·G6P, or the G2P·G1P·G6P complexes (Fig. 5*A*).

To address whether any modification on the ATP binding pocket of G2P might also affect its endonuclease activity, ATPase and nuclease assays were performed. As revealed in Fig. 5*B*, 20 μM Myr reduces the G2P ATPase activity to nearly background levels and exerts a 50% inhibition on the nuclease activity of G2P.

The G1P modulator exerts a negative effect in the G2P endonuclease and enhances its ATPase activity (6). To learn if the G1P presence affects the action of Myr on G2P we have measured the activities associated with the G1P·G2P complex. G1P, at a concentration that stimulates the ATPase activity and reduces ~50% the G2P nuclease, was preincubated with G2P, then incubated with Myr and ATPase, and nuclease assays were performed. Myr inhibits the G1P stimulatory effect on the G2P ATPase activity, but is not able to inhibit the G2P nuclease activity (Fig. 5*C*). This is consistent with the observation that Myr (50 μM) is unable to disrupt the G1P·G2P complex, as addressed by protein-protein cross-linking in the presence of increasing concentrations of Myr (data not shown). Furthermore, in the presence of Ca^{2+}, G2P binds to DNA, and such a binding is reduced by the addition of 20 μM Myr (data not shown). It is likely, therefore, that Myr introduces a conformational change in the G2P catalytic domain of the G2P ATPase and affects both the ATPase and nuclease activities in a manner that is different from the G1P-induced conformational change.

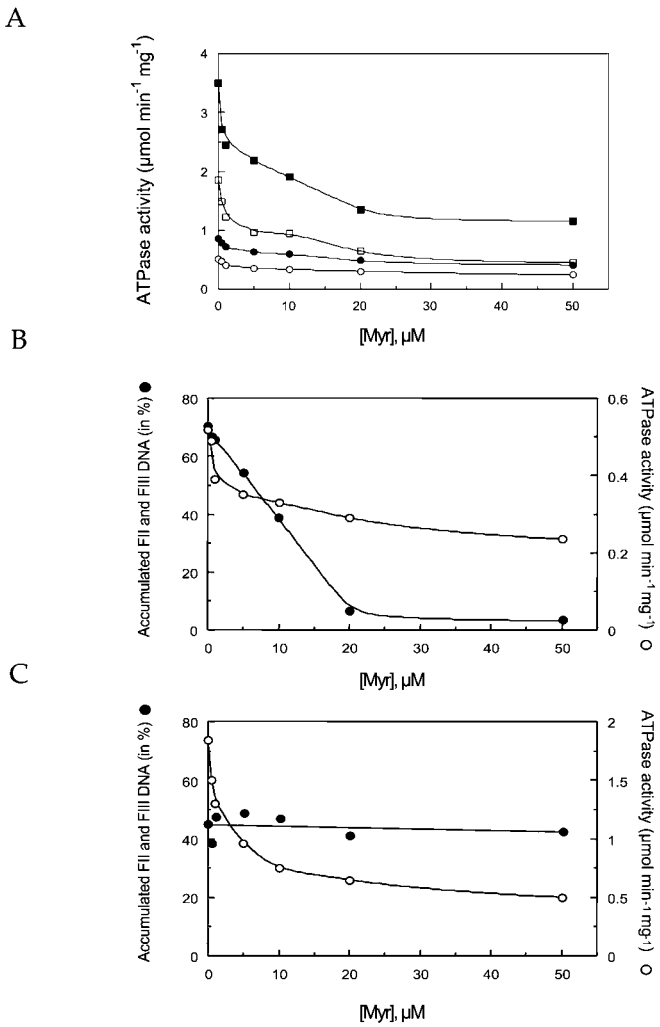

FIG. 5. **Myr affects the ATPase and endonuclease activities of G2P.** *A*, G2P (20 nM) alone or preincubated with G*1*P (160 nM), G*6*P (160 nM), or both G*1*P and G*6*P for 5 min was then incubated with increasing concentrations of Myr (0.5, 1, 10, 20, and 50 μM). The ATPase assay was performed as described under "Experimental Procedures," with 5 mM ATP (0.05 μCi/nmol). The ATPase activity of G2P (*empty circles*), G2P + G6P (*filled circles*), G2P + G*1*P (*empty squares*) and G2P + G*6*P + G*1*P (*filled squares*) was assayed. *B*, G2P (20 and 80 nM for ATPase and nuclease assays) was incubated with supercoiled pCB363 DNA (20 nM) or 5 mM ATP (0.05 μCi/nmol) and then with increasing concentrations of Myr (0.5, 1, 10, 20, and 50 μM). The endonuclease (*filled circles*) and ATPase (*empty circles*) of G2P was assayed. In *C*, G2P (20 and 80 nM for ATPase and nuclease assays, respectively) was preincubated with G*1*P (160 nM) and with supercoiled pCB363 DNA (20 nM) or 5 mM ATP (0.05 μCi/nmol) and then with increasing of Myr (0.5, 1, 10, 20, and 50 μM). The endonuclease (*filled circles*) and ATPase (*empty circles*) activities of G2P were assayed.

DISCUSSION

The mechanism by which viruses translocate their genome into empty procapsids is still not understood. The translocation of SPP1 concatemeric dsDNA into a preformed viral capsid is a complex process that requires the concerted action of the terminase-DNA complex with the portal protein located at a unique vertex of the procapsid. This is consistent with the observation that: (i) *in vivo*, cleavage at *pac* is independent of G*6*P, but it is stimulated by its presence (5) and (ii) the purified major capsid, G*13*P, scaffolding, G*11*P, and accessory, G7P, procapsid protein are unable to interact with the terminase (19, 23, 27).

In many phage systems, the terminase large subunit physically interacts with the portal protein. Previously, we have failed to detect a G2P·G*6*P stable complex in solution (19, 6) but the enzymatic data shown here demonstrate an interaction between both proteins. Using different approaches, it is suggested that *G1*P physically interacts with *G6*P. We showed that *G1*P·*G6*P synergistically increases the V_{max} of the G2P ATPase. The ATPase activity associated with the terminase is likely to power DNA translocation in the SPP1 DNA packaging motor.

The major finding presented in this report is the regulation of the terminase ATPase activity by the portal protein G*6*P. G*6*P, which neither binds ATP nor hydrolyzes ATP on its own, stimulates by 2-fold the ATPase activity of G2P. This is consistent with the observation that no ATPase activity has been associated with any of the portal proteins described so far and with a 1.2-fold stimulation of the T4 gp17 ATPase by the addition of the gp20 portal protein (17).

*G1*P, which binds but does not hydrolyze ATP, might induce a conformational change on G2P. This postulated allosteric change in G2P leads to a stimulated ATPase and markedly reduced ATP-independent endonuclease, but does not affect sequence-independent DNA binding activity of G2P in the G*1*P·G2P complex, at any region other than at the *pac* site (6). This is consistent with the observation that both G*1*P and Myr modified the activities associated with G2P in a different manner.

*G6*P stimulates the G2P ATPase activity, but neither alters the endonuclease nor the DNA binding activity of G2P. In the presence of a large excess of G*1*P ($G2P_1$·$G1P_{>6}$·$G6P_1$), both ATPase and endonuclease activities associated with G2P are drastically reduced, and a large excess of G*6*P reduced the G2P ATPase activity. Since the presence of an excess of G*6*P cannot reverse the negative effect of G*1*P on the endonuclease activity of terminase by titrating out G*1*P, but reduces the ATPase activity (Fig. 4*B*), we have to assume that both G*1*P and G*6*P are bound to G2P and act as modulators of the G2P activities. The global analysis of the ATP hydrolysis data showed that the most active ATPase species seems to have a $G2P_1$·$G1P_2$·$G6P_1$ or $G2P_1$·$G1P_3$·$G6P_1$ stoichiometry. The k_{cat} is significantly reduced at higher G*6*P or G*1*P concentrations. On the basis of these data, we suggest that G*1*P and G*6*P are involved in promoting a conformational switching in G2P, thus performing a reorganization of the terminase subunits assembled at the procapsid to yield a catalytically competent DNA packaging motor complex with reduced endonuclease activity.

The experimental data regarding ATPase activity demonstrated that the K_m and k_{cat} had changed significantly in the presence of G*1*P and G*6*P. The affinity toward ATP has increased in the presence of both proteins, as observed by a decrease of 4-fold in the K_m of the $G2P_1$·$G1P_2$·$G6P_1$ complex. At the same time, there is an increase of 13-fold in the turnover rate (k_{cat}) of the G2P ATPase.

Studies on phage ϕ29 and T3 packaging systems have demonstrated that 2 bp of DNA are packaged per ATP hydrolyzed (28, 29). If we assumed that this ATP hydrolytic requirement applies to SPP1, the catalytic capacity of the $G2P_1$·$G1P_2$·$G6P_1$ complex (350–380 ATP min^{-1}) is ~10-fold lower than expected for the packaging of the 45.9-kb SPP1 chromosome in ~6 min. The ATPase activity, however, could be different *in vivo*, when a 12-mer G*6*P is embedded within the procapsid context, and when concatemeric DNA is present. The packaging motor has to possess a turnover rate of at least 3,800 min^{-1}, similar to the one observed for the hexameric DnaB replicative helicase (k_{cat} 2,700–4,100 min^{-1}) (30). For DNA helicases, the amount of DNA that can be unwound from the free energy derived from the hydrolysis of one molecule of ATP is limited thermodynamically to no more than 5 bp (31). At present, the translocating step size of the SPP1 packaging motor is unknown.

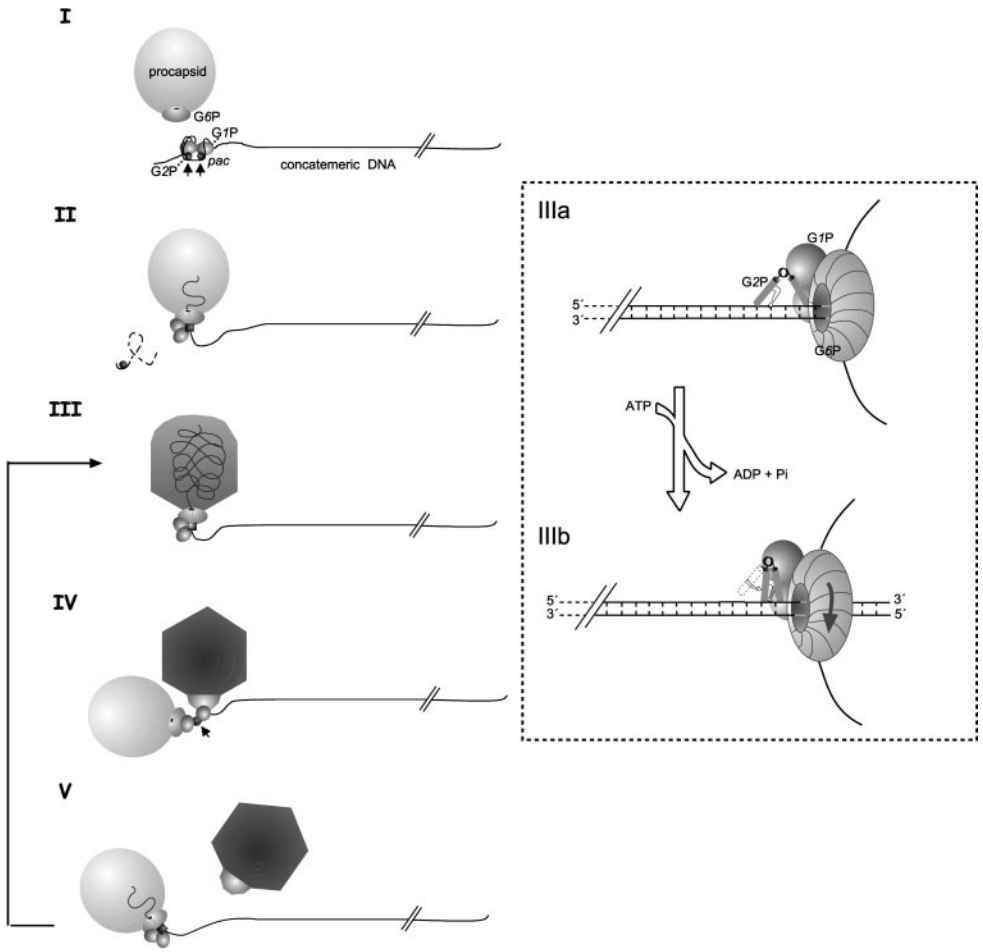

FIG. 6. **SPP1 DNA packaging model.** The different steps of the packaging process are denoted in Roman numerals. The proposed conformational switching of monomeric G2P and dodecamer G6P are depicted in the scheme by the *same color but different shapes*. The conformational changes of the procapsid are depicted by different *shades of color* (the increase in darkness correlate with DNA packaging). *Arrows* point out endonucleolytic cleavage by G2P. The two G1P decamers are denoted as *spheres*. The picture enclosed shows the mechanism resembling the inchworm model initially described for DNA helicases and proposed for the SPP1 terminase (see text for details).

Previously, we have proposed that G1P induces a conformational change in G2P, with "modified G2P" having a stimulated ATPase and a shut off of endonuclease activity (6). The experiments reported here show that Myr inhibits the endonuclease and ATPase activities of G2P, whereas Myr exerts a negative effect on the ATPase but does not seem to affect the nuclease activity of the G2P·G1P complex. Similar results are observed if G6P is added to the reaction G1P·G2P complex. It is likely, therefore, that the nuclease and ATPase of G2P are present in discrete and related modules, but the presence of G1P uncoupled such domain interaction. This is consistent with T4 terminase mutants that showed a defect as a translocase but not in terminase cutting activity (16).

A Model for SPP1 DNA Packaging—The SPP1 packaging motor is a highly specific and processive enzyme starting within a concatemeric DNA substrate, which is able to translocate as many as 183.6-kb (4 processive headful packaging events) for an initial binding to the *pac* site (5, 18). The overall process begins with replication of the viral genome to generate head-to-tail concatemeric dsDNA. It is generally accepted that DNA translocation into the procapsid is powered by ATP hydrolysis; however there is much less agreement what general mechanism of ATP hydrolysis drives DNA into the procapsid (reviewed in Refs. 1–4). Unlike the ϕ29 packaging motor, that is composed of twelve subunits of the portal, five or six pRNA and ATPase molecules (32–34), in SPP1 the packaging motor is composed of twelve subunits of G6P, more than one decameric G1P and a monomeric G2P (Refs. 8, 6, 10, and this work). At least in the SPP1 case the presence of the pRNA in the packaging motors has been ruled out (see Ref. 9).

After Hendrix (35), Dube *et al.* (11), Simpson *et al.* (33), and Guasch *et al.* (34), we propose a model for SPP1 DNA packaging that might apply to other bacteriophages and to herpesviridae. This is schematically depicted in Fig. 6.

I) Interaction of the Terminase with Concatemeric DNA—Specific recognition and endonucleolytic cleavage of the SPP1 *pac* sequence is the first step in DNA packaging. It requires exclusively two terminase subunits, although the terminase activity is enhanced by the presence of the portal protein (5, 6). Biochemical evidence shows that two molecules of G1P bind specifically and cooperatively to *pac*L and *pac*R subsites and interact and hold the two subsites together in a DNA loop containing the *pac*C subsite on a concatemeric substrate (Ref. 8, Fig. 6, *step I*). G1P loads G2P at each of the two b-boxes. G2P introduces an ATP-independent cut at each b-box, forming the nicking complex (6). The close interaction between the G1P oligomer bound at *pac*R and G2P positioned at its proximal b-box (see Fig. 1*A*) might favor the formation of the "modified" $G1P_2{\cdot}G2P_1$ at *pac*R. The modified $G1P_2{\cdot}G2P_1$ terminase has a shut off endonuclease activity and an activated ATPase activity (6). The G2P molecule, which had cleaved the b-box distal from the *pac*R subsite, now freed from G1P, initially bound to *pac*L and will degrade the non-encapsidated DNA end in a *pac*-independent manner (Refs. 5, 6, and 13 and Fig. 6, *step II*). This

observation imparts the unique directionality of the SPP1 packaging process. The G*1*P_2·G2P_1 complex bound to the DNA end carrying *pac*R is proposed to bind G*6*P localized at the portal vertex of the empty procapsid to initiate processive translocation of SPP1 DNA (Fig. 6, *step II*).

II) Interaction of the Terminase-DNA Complex with the Procapsid and Subsequent Transition to a Further Activated ATPase Complex—The interaction of G2P_1·G*1*P_2-*pac*R DNA (postcleavage complex) with G*6*P, at a unique vertex of the procapsid, should activate the ATPase activity that powers DNA packaging even more. Indeed, the G2P_1·G*1*P_{2-3}·G*6*P_1 complex increased the ATP affinity (K_m of 219 μM) and turnover (k_{cat} of 366 min^{-1}) of G2P (Tables I and II). There are no direct data on the location of G2P, although in Fig. 6, *step II*, we assumed that one G2P monomer is interacting stably with two G*1*P decamers and transiently with one G*6*P dodecamer.

III) Transition to an Active DNA Packaging Machine That Translocates DNA into the Procapsid Interior—The catalytically competent G2P_1·G*1*$P_{>1}$·G*6*P_1-DNA packaging motor is believed to provide the energy for the linear translocation of DNA into the procapsid initiated by entry of the *pac*R DNA end. The DNA is pumped through the G*6*P pore until a threshold amount of DNA (headful) is reached inside the procapsid (5, 8, 13, 18, 22). Models for this DNA translocation mechanism normally take into consideration the symmetry mismatches between components of the DNA translocation machinery (between the procapsid and portal protein, or between procapsid, portal protein, and DNA, or between the portal protein, the terminase, and DNA) that would permit rotations between the components of the DNA translocation machinery (32–35). This rotation would be associated to sequential firing of the oligomeric terminase ATPase activity providing energy for a conformational change in one or in a few portal protein subunits that generates the power stroke for mechanical translocation of DNA to the capsid interior (33, 34).[3] Although these models provide interesting test cases, direct evidence of rotation between components of the packaging machinery or the possibility that the portal protein is the mechanical device of the packaging machinery still lacks experimental proof.

It is difficult to envision how a portal protein rotary motion as described in the above packaging models could accommodate the observation that the SPP1 packaging ATPase is composed of one monomer of G2P, two or more decamers of G*1*P, and one dodecamer G*6*P (G2P_1·G*1*$P_{>1}$·G*6*P_1) (Ref. 6 and this work). We propose here a model in which the G2P_1·G*1*$P_{>1}$·DNA complex binds to G*6*P_1 embedded in the procapsid. The docking of the terminase-DNA complex at G*6*P might place the DNA end at the portal protein central channel. The ATP hydrolysis leads to a conformational change in G2P driving net translocation of DNA to the procapsid interior and "loose" grip of G2P on the DNA followed by a new translocation step (Fig. 6, *stage IIIa* and *IIIb*). This mechanism resembles the inchworm model initially described for DNA helicases (reviewed in Ref. 36). The G2P conformational change would provide energy for a conformational change in one or in a few portal protein subunits that might induce rotation of the portal and help in the mechanical translocation of the DNA. The structural organization of the G2P_1·G*1*$P_{>1}$·G*6*P_1 complex at the procapsid portal vertex would ensure processivity of the reaction preventing G2P to fall off from the nucleoprotein complex during successive translocation steps.

DNA packaging leads to a drastic conformational change of the SPP1 major capsid protein, from a roundish procapsid structure to a capsid lattice, with sharp angles that highlight its icosahedral organization (Fig. 6, *steps II* and *III*).

IV) Transition to an Activated Cleavage Complex—When a threshold amount of DNA, representing about 103% of the SPP1 genome, has been packaged (headful), G2P shifts from translocase to a less specific endonuclease with a subsequent halt in DNA packaging. We could envisage that once the procapsid is full, G*6*P acting as a gauge (24) might loose affinity for G*1*P. G*1*P of the G2P_1·G*1*$P_{>1}$·G*6*P_1 interacts with G*6*P of another spherical procapsid and promotes a change in the stoichiometry of the G2P_1·G*1*$P_{>1}$·G*6*P_1 packaged complex toward the G2P_1·G*1*P_1·G*6*P_1 complex. The latter complex has low ATPase and a *pac*-independent cleavage activity with a subsequent release of DNA from the mature capsid. Alternatively, upon procapsid expansion G*6*P is unable to interact with the terminase; hence indirectly reducing the velocity of packaging or increasing the energy required to continue DNA packing, which might attenuate translocation and by an unknown mechanism activate the G2P endonuclease activity. This is consistent with the observation that the efficiency of DNA packaging in SPP1*siz* mutant, which leads to undersizing of the DNA packaged, is reduced. It was shown that the SPP1*siz* mutations map in gene *6* coding for G*6*P and suggested that a trigger for headful cleavage could be the incapacity of the packaging machinery to encapsidate further DNA into the procapsid (22).

V) Termination of Packaging—DNA packaging terminates when the DNA inside the capsid is separated from the concatemer by a cutting process. The headful cleavage generates a new end, to which the packaging motor remains bound, serving as the starting point for the second round of DNA packaging (13, 5, 18, 22).

Acknowledgment—We thank A. A. Antson for the communication of unpublished results and discussions on this manuscript.

[3] A. Antson and P. Tavares, personal communication.

REFERENCES

1. Black, L. W. (1989) *Annu. Rev. Microbiol.* **43,** 267–292
2. Catalano, C. E., Cue, D., and Feiss, M. (1995) *Mol. Microbiol.* **16,** 1075–1088
3. Fujisawa, H., and Morita, M. (1997) *Genes Cells* **2,** 537–545
4. Catalano, C. E. (2000) *Cell Mol. Life Sci.* **57,** 128–148
5. Chai, S., Bravo, A., Lüder, G., Nedlin, A., Trautner, T. A., and Alonso, J. C. (1992) *J. Mol. Biol.* **124,** 87–102
6. Gual, A., Camacho, A. G., and Alonso, J. C. (2000) *J. Biol. Chem.* **275,** 32311–32319
7. Bravo, A., Alonso, J. C., and Trautner, T. A. (1990) *Nucleic Acids Res.* **18,** 2881–2886
8. Chai, S., Lurz, R., and Alonso, J. C. (1995) *J. Mol. Biol.* **252,** 386–398
9. Dröge, A., and Tavares, P. (2000) *J. Mol. Biol.* **296,** 103–115
10. Lurz, R., Orlova, E. V., Gunther, D., Dube, P., Dröge, A., Weise, F., van Heel., M., and Tavares, P. (2001) *J. Mol. Biol.* **310,** 1027–1037
11. Dube, P., Tavares, P., Lurz, R., and van Heel, M. (1993) *EMBO J.* **12,** 1303–1309
12. Chai, S., Kruft, V., and Alonso, J. C. (1994) *Virology* **202,** 930–939
13. Deichelbohrer, I., Messer, W., and Trautner, T. A. (1982) *J. Virol.* **42,** 83–90
14. Chai, S., and Alonso, J. C. (1996) *Nucleic Acids Res.* **24,** 282–288
15. Leffers, G., and Rao, B. V. (2000) *J. Biol. Chem.* **275,** 37127–37136
16. Rao, V. B., and Mitchell, M. S. (2001) *J. Mol. Biol.* **314,** 401–411
17. Baumann, R. G., and Black, L. W. (2003) *J. Biol. Chem.* **278,** 4618–4627
18. Tavares, P., Lurz, R., Stiege, A., Rückert, B., and Trautner, T. A. (1996) *J. Mol. Biol.* **264,** 954–967
19. Gual, A., and Alonso, J. C. (1998) *Virology* **242,** 279–287
20. Steven, A. C., Trus, B. L., Maizel, J. V., Unser, M., Parry, D. A. D., Wall, J. S., Hainfeld, J. F., and Studier, F. W. (1988) *J. Mol. Biol.* **200,** 351–365
21. Ayora, S., Rojo, F., Ogasawara, N., Nakai, S., and Alonso, J. C. (1996) *J. Mol. Biol.* **256,** 301–318
22. Tavares, P., Santos, M., Lurz, R., Morelli, G., de Lencastre, H., and Trautner, T. A. (1992) *J. Mol. Biol.* **225,** 81–92
23. Gual, A. (1998) *Characterization of Bacillus subtilis Bacteriophage SPP1 Terminase Enzyme.* Ph.D. Dissertation, Universidad Autónoma de Madrid, Spain
24. Orlova, E., Dube, P., Beckmann, E., Zemlin, F., Lurz, R., Trautner, T. A., Tavares, P., and van Heel, M. (1999) *Nat. Struct. Biol.* **6,** 842–846
25. Walker, E. H., Pacold, M. E., Perisic, O., Stephens, L., Hawkins, P. T., Wymann, M. P., and Williams, R. L. (2000) *Mol. Cell.* **6,** 909–919
26. Xu, H., Ziegelin, G., Schroder, W., Frank, J., Ayora, S., Alonso, J. C., Lanka, E., and Saenger, W. (2001) *Nucleic Acids Res.* **29,** 5058–5066
27. Becker, B., de la Fuente, N., Gassel, M., Gunther, D., Tavares, P, Lurz, R., and Alonso, J. C. (1997) *J. Mol. Biol.* **268,** 822–839
28. Guo, P., Erickson, S., and Anderson, D. L. (1987) *Science* **236,** 690–694

29. Shibata, H., Fujisawa, H., and Minagawa, T., (1987) *J. Mol. Biol.* **20,** 845–851
30. Arai, K., and Komberg, A. (1981) *J. Biol. Chem.* **256,** 5253–5259
31. Lohman, T. M., and Bjornson, K. P. (1996) *Annu. Rev. Biochem.* **65,** 169–214
32. Ibarra, B., Caston, J. R., Llorca, O., Valle, M., Valpuesta, J. M., and Carrascosa, J. L. (2000) *J. Mol. Biol.* **298,** 807–815
33. Simpson, A. A., Tao, Y., Leiman, P. G., Badasso, M. O., He, Y., Jardine, P. J., Olson, N. H., Morais, M. C., Grimes, S., Anderson, D. L., Baker, T. S., and Rossmann, M. G. (2000) *Nature* **408,** 745–750
34. Guasch, A., Pous, J., Ibarra, B., Gomis-Rüth, F. X., Valpuesta, J. M., Sousa, N., Carrascosa, J. L., and Coll, M. (2002) *J. Mol. Biol.* **315,** 663–676
35. Hendrix, R. W. (1978) *Proc. Natl. Acad. Sci. U. S. A.* **75,** 4779–4783
36. Soultanas, P., and Wigley, D. B. (2001) *Trends Biochem. Sci.* **26,** 47–54